Complete and incomplete fusion reactions in $^{12}C+^{89}Y$: Excitation functions and recoil range measurements

B. Bindu Kumar and S. Mukherjee
School of Studies in Physics, Vikram University, Ujjain 456010, India

S. Chakrabarty, B. S. Tomar, A. Goswami, and S. B. Manohar
Radiochemistry Division, Bhabha Atomic Research Centre, Mumbai 400085, India
(Received 11 September 1997)

Excitation functions and recoil range distributions for radioactive products formed in the reactions of ^{12}C on ^{89}Y have been measured using catcher foil technique followed by gamma-ray spectrometry. The alpha emission products show higher cross sections than that predicted for complete fusion. Recoil range distributions of evaporation residues indicate incomplete momentum transfer events. Detailed Monte Carlo simulation of the shapes of recoil range distributions for these processes have been carried out using PACE2 code to extract the contributions of incomplete fusion in the individual channels. From the relative yields of incomplete fusion products the excitation energy and angular momentum of the incompletely fused composite nucleus have been deduced. The values agree well with the break-up fusion model of the incomplete fusion.
[S0556-2813(98)03102-1]

PACS number(s): 25.70.Jj, 25.70.Gh

I. INTRODUCTION

The study of heavy ion fusion reactions has been the subject of interest for the past three decades. The fusion cross sections as a function of entrance channel mass asymmetry, center of mass energy and angular momentum have been explained in terms of the model based on interaction barrier, critical angular momentum and critical distance of approach [1]. As the projectile energy is increased compound nucleus formation is hindered and incomplete fusion (ICF) starts competing with complete fusion (CF). In ICF reaction, only a part of the projectile fuses with the target accompanied by the emission of light ejectiles at forward angles with approximately beam velocity. These ICF reactions were first observed by Britt and Quinton [2] and Galin *et al.* [3]. The study of ICF by particle-gamma coincidence studies [4] contributed to the understanding of the mechanism of these reactions. As the projectiles ^{12}C, ^{16}O are clusters of α particles, it could be assumed that it is easy to transfer an α particle from these projectiles to the target. In such reactions the mass flow is always from projectile to target.

Several models have been proposed to explain the ICF reactions, such as break-up fusion [5], hot spot [6], sum rule model [7], promptly emitted particles [8] and exciton model [9]. All these models have been used to fit the experimental data obtained using projectile energies above 10 MeV/nucleon. However, some recent studies showed the onset of ICF just above the Coulomb barrier. Parker *et al.* [10] observed forward peaked alpha particles in reactions of 6 MeV/nucleon ^{12}C on ^{51}V. Morgenstern *et al.* [11] observed ICF components in the velocity spectra of evaporation residues (ER's) in a reaction of ^{40}Ar with boron and carbon targets. Tserruya *et al.* [12] found evidence for ICF from time-of-flight measurements of ER's in a reaction of 5.5 to 10 MeV per nucleon ^{12}C with ^{120}Sn, ^{160}Gd, and ^{197}Au. Tomar *et al.* by their excitation functions [13] and recoil range distribution studies [14] have clearly shown the significant contribution of ICF in the cross section of α emission channels as well as α transfer products.

The recoil range distribution (RRD) of the heavy residues depends on the momentum transferred in the reaction. In the ICF process the momentum transferred is proportional to the mass of the projectile fragment fusing with the target nuclei. Measurement of recoil range can also be used in distinguishing different ICF processes in lighter systems where the same product may be formed by more than one fusion process, followed by different degrees of particle emission. On the other hand in TOF studies [15] only the mass of the residue is identified and not its atomic number. The particle gamma coincidence [4] measurements on the other hand are useful for the heavier system where the evaporation of charged particle is hindered by the Coulomb barrier. There have been conflicting reports about the angular momenta involved in ICF. The γ-multiplicity measurements by Inamura *et al.* [4], Wilczynski *et al.* [7], and Trautmann *et al.* [16] showed that ICF involves l values more than l_{CR}. However a few studies [17] on spherical targets showed involvement of l values lower than l_{CR}. This suggests that ICF may be competing with CF even at l values lower than l_{CR} contrary to the hypothesis of angular momentum window in the sum rule model of ICF.

In the present work we measured the excitation functions $[\sigma(E)]$ of the various radionuclides formed in the reaction of ^{12}C on ^{89}Y in beam energy range 70–87 MeV and RRD at 84 MeV ^{12}C beam energy. Detailed modeling of the RRD's, based on data from complimentary studies of excitation functions will help in separating the contributions of CF and ICF process in each reaction channel and thereby one can estimate the cross sections of various fusion processes in the total reaction cross section. In order to identify the yields

TABLE I. Nuclear spectroscopic data used in this work [20].

Nuclide	Spin	Half-life	E_γ (keV)	I_γ (%)
^{98}Rh	2^+	9.05*m*	652	94.2
^{97}Rh^m	$1/2^-$	44.3*m*	188	51.2
^{97}Rh^g	$9/2^+$	31.1*m*	421	75.0
^{96}Rh	5^+	9.89*m*	832	100
^{97}Ru	$5/2^+$	2.9*d*	215	85.8
^{95}Ru	$5/2^+$	1.64*h*	336	100
^{96}Tc^g	7^+	4.28*d*	778	100
^{95}Tc^g	$9/2^+$	20 *h*	765	93.9
^{94}Tc^g	7^+	4.9*h*	871	100
^{93}Tc^g	$9/2^+$	2.75*h*	1363	65.8
^{93}Mo^m	$21/2^+$	6.85*h*	685	99.7
^{92}Nb^m	2^+	10.15*d*	934	100
^{90}Nb^g	8^+	14.6*h*	1129	92.66

associated with CF and ICF the observed RRD's are compared with the predictions of Monte Carlo simulations using the code PACE2 [18]. The results obtained in the present work are discussed in terms of the breakup fusion model of ICF. The relative yields of various ICF products have been used to deduce the angular momenta involved in ICF.

II. EXPERIMENTAL PROCEDURE

A. Excitation functions

The excitation functions for production of twelve radionuclides from the reaction ^{12}C+^{89}Y were measured at incident ^{12}C energies up to 87 MeV. The experiments were carried out at the BARC-TIFR Pelletron accelerator at Mumbai, India. Stacks consisting of two self-supporting targets of yttrium (1 mg/cm^2) separated by aluminum foils (2 mg/cm^2) were bombarded with ^{12}C beam. Three irradiations were carried out for each such stack of target and degraders encompassing the beam energy between 70 and 87 MeV for ^{12}C. The energies at the target are the average values of the incident and outgoing projectile energies. The beam energy degradation in each target foil was calculated using the stopping power tables of Northcliffe and Schilling [19]. The irradiation time of around 2 h was selected according to the half lives of the radioisotopes produced. The total charge collected for each irradiation was around 700 μC. This was measured using an electron suppressed Faraday cup placed behind the target assembly. The radionuclides generated in each target catcher assembly were then identified by counting the foils successively on a precalibrated 60 cc HPGe detector coupled to a 4 K MCA. The efficiency of the detector as a function of gamma ray energy had been determined using a standard ^{152}Eu source. The detector resolution was 2 keV at 1332 keV. Each foil was counted for 300 seconds duration immediately after activation. Subsequently, the foils were recounted for successively longer durations over a period of two weeks.

The yields of the radioinuclides identified in each foil were determined using the published half-lives, gamma-ray energies and branching ratios [20]. Table I lists the nuclear spectroscopic data for the nuclides for which the excitation functions were measured in this work. The computer code SAMPO was used to find the areas of the peaks in the gamma-ray spectra. From the measured count rate CR(t) at any time t, the cross sections (σ) were calculated using the standard relation,

$$\mathrm{CR}(t) = N\phi\sigma(1-e^{-\lambda T_i})e^{-\lambda t}\varepsilon_\gamma I_\gamma, \tag{1}$$

where N is the number of atoms/cm^2 in target, ϕ is the intensity of incident particles, T_i and t are the bombardment and cooling time, λ is the decay constant of the radionuclide, and ε_γ and I_γ are the detection efficiency and branching intensity of the gamma ray, respectively. In the case of the radionuclides such as ^{97}Ru, ^{95}Tc the measured cross sections are the cumulative values. The corrections for the precursor contribution was carried out by subtracting the precursor cross section measured independently. Many of the radionuclides studied have isomeric states with decay properties different from the ground state. In the case of ^{97}Rh it was possible to measure the two isomers, while in some cases (e.g., ^{92}Nb) the decay schemes of one of the isomers was not suitable for measurements. In some cases (^{96}Tc, ^{90}Nb) where the isomeric state decays to ground state the measured yields include both states.

B. Recoil range distributions

Recoil range distributions for a number of radioactive products of the reactions of ^{12}C on ^{89}Y, recoiling into aluminum, were measured at ^{12}C beam energy of 84 MeV. The target consisted of approximately 100 μgm/cm^2 yttrium evaporated onto a thin aluminum foil of thickness 100 μgm/cm^2. The target was mounted with the aluminum backing facing the beam, so that the catcher stack immediately followed the yttrium layer. The catchers used were evaporated aluminum foils, typically 100 μgm/cm^2 thick. The thickness of each catcher foil was measured prior to its use, with an uncertainty of $<5\%$, by measuring the energy loss suffered in the foil by 5.486 MeV α particle from a ^{241}Am source. The stopping power values of Northcliffe and Schilling [19] for the stopping of α particle in aluminum were used for determining the thickness.

The target and a stream of 12 catcher foils were mounted on annular holders with internal diameter of 12 mm, in a close geometry inside the irradiation chamber. The beam current was measured with an electron suppressed Faraday cup placed behind the target-catcher assembly. The ^{12}C beam was collimated to a spot of 2 mm, and the stack was irradiated for 18 h with a fluence of about 1000 μC. After the irradiation, the activities of individual reaction products were measured by following the gamma activities of the individual catcher foils for a period of two weeks. The cross sections (σ) for a particular reaction product in different foils were obtained using Eq. (1).

The yield distribution as a function of depth in the catcher stack was obtained for each product by dividing the yield in each catcher by its measured thickness and plotting the resulting yield against cumulative catcher thickness to obtain the RRD. The accuracy of these distributions was limited by the uncertainty in determining the catcher thickness, generally about 5%. No attempt was made to obtain absolute cross section in this measurement, which simply determined the shape of each recoil. The recoil distributions were normal-

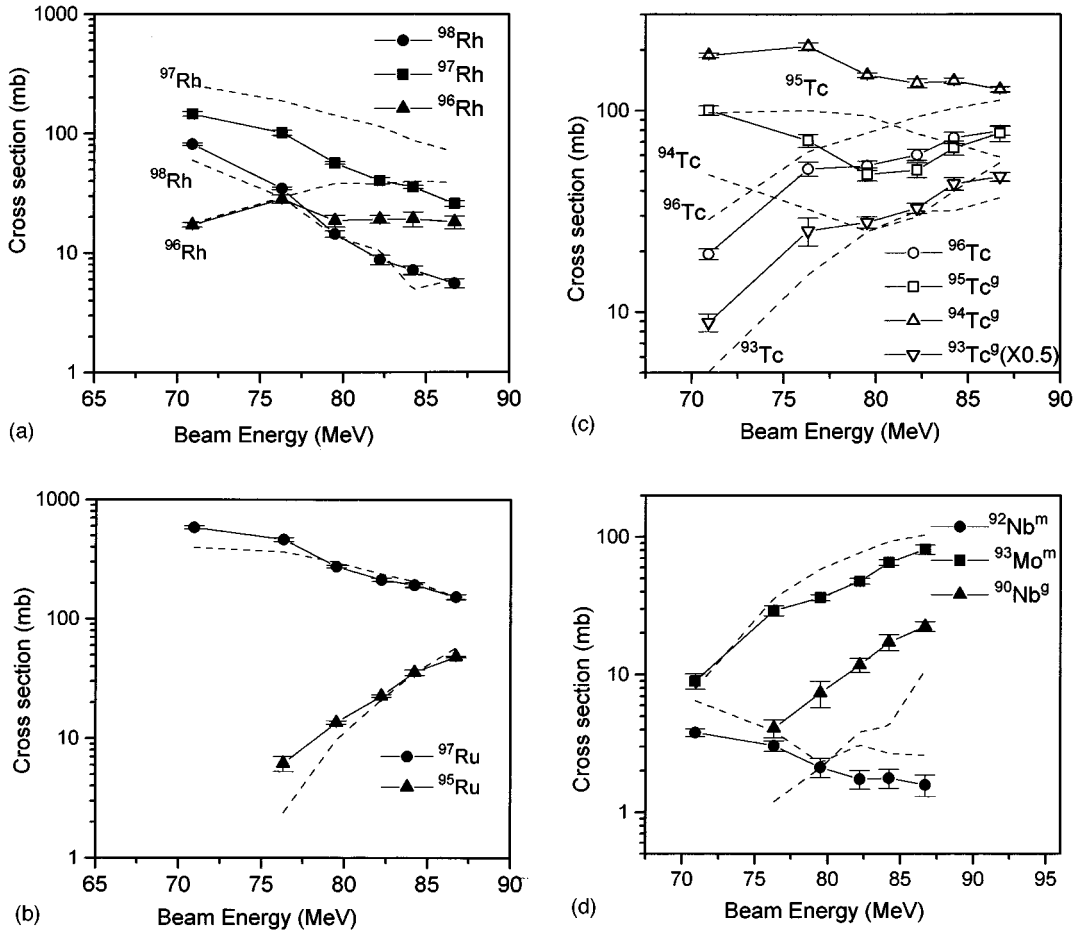

FIG. 1. (a)–(d) Excitation functions of evaporation residues in $^{12}C+^{89}Y$. The solid lines are an eye guide to the experimental data. The dashed lines represent the PACE2 predictions for CF formation of ER's.

ized using the cross section obtained in the excitation function measurements discussed in Sec. II A.

III. ANALYSIS OF THE EXPERIMENTAL DATA

Figures 1(a)–1(d) show the measured excitation functions of the twelve evaporation residues. The experimentally measured ER's are indicated by various symbols and solid lines through these points are just eye guide. The errors on the cross sections are approximately 10–15% which arises mostly from the counting statistics, detector efficiency, target thickness and γ ray intensity values. The theoretical estimate of the cross sections were obtained using the Monte Carlo simulation code PACE2 [18] with KRK formula for level density [21]. The optical model parameters for emitted light particles were taken from Perey and Perey [22] for alphas, protons and neutrons. The average gamma transition strengths compiled by Endt [23] were used for the present work. The KRK prescription takes into account the excitation energy dependence of the level density parameter ''**a**''. In the present calculations for ER excitation functions, the value of ''**a**'' used was $A/8$. The other input parameters in the programme were used as default values. The calculated excitation functions are shown as dashed lines.

The RRD's for various reaction products, studied in the present work, are shown in Figs. 2(a)–2(b). The solid lines are eye guides to the experimental points. The abscissa in the figures represents the range projected along the beam axis. The error on the cross section data is of the order of 10–15 %, which is primarily due to the counting statistics. The RRD's for the ER's formed by CF were simulated using the code PACE2 with the input parameter as discussed above. The code calculates the double differential cross section $(d^2\sigma/dEd\Omega_{\rm lab})$ for ER's which was transformed into the projected range distribution along the beam axis using the range energy table of Northcliffe and Schilling [19]. The RRD's obtained by the PACE2 code were normalized to the experimental RRD's by adjusting the height and keeping the peak position and width constant. In Figs. 2(a) and 2(b) the RRD's for the ER's obtained by PACE2 are shown by solid curves. The dashed curves are the ICF components obtained by subtracting the CF contributions from the experimental curves.

IV. RESULTS AND DISCUSSION

A. Excitation functions

The experimental results for various reaction channels, along with their predicted cross sections with PACE2 code are shown in Figs. 1(a)–1(d). The excitation functions for the rhodium products produced through xn channels of the $^{12}C+^{89}Y$ compound system are shown in Fig. 1(a). It can be seen that the excitation function for the product ^{98}Rh is in

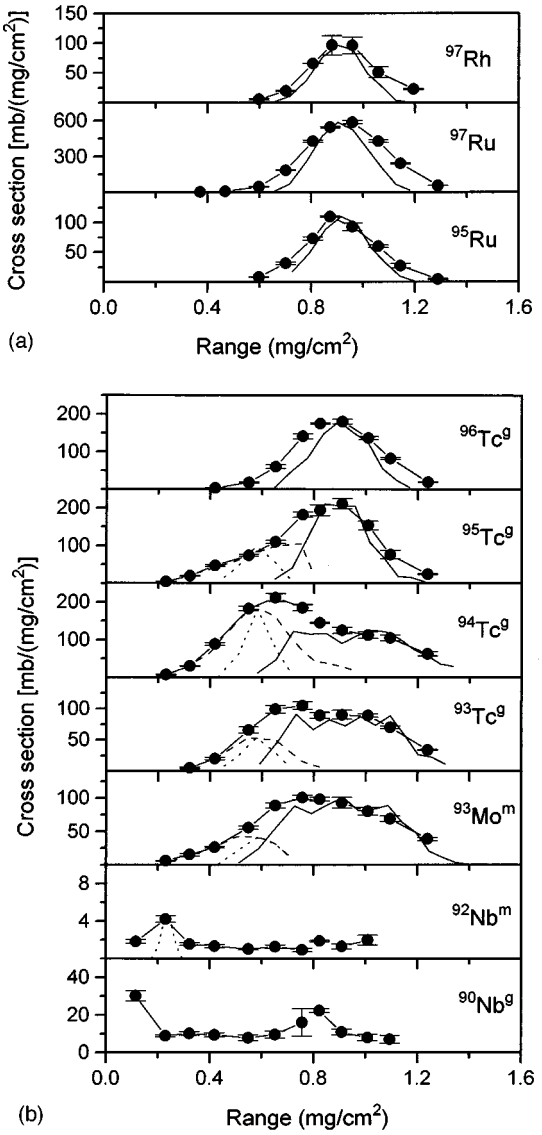

FIG. 2. (a) and (b) Recoil range distributions of evaporation residues in $^{12}C+^{89}Y$. The continuous lines are the PACE2 predictions for CF formation of ER's. The dashed lines represent the ICF component obtained by subtracting the PACE2 predictions from the experimental data. Dotted lines are the simulated RRD's for ICF based on breakup fusion model.

agreement with the theoretical predictions. This is quite obvious, as the rhodium products are formed from the CF of ^{12}C with ^{89}Y. Surprisingly, there is a disagreement by a factor of 2 between the theory and experiment for the product ^{97}Rh for the entire region up to 86 MeV and for the product ^{96}Rh beyond 75 MeV. Figure 1(b) shows the experimental and theoretical excitation functions for the ^{97}Ru and ^{95}Ru products. The dotted curves correspond to the PACE2 calculations. As expected, the calculated values agree well with the experimental results, thereby showing that the Ru products are formed via pxn channels after the CF of ^{12}C with ^{89}Y. From Figs. 1(a) and 1(b) it can be seen that xn and pxn products are formed via deexcitation of the CN formed in CF. There is agreement between the experimental and theoretical values in four out of the five evaporation residues. In view of the statistical nature of the calculations this can be considered as a fairly satisfactory result.

The excitation functions for Tc products are shown in Fig. 1(c). It can be seen from the figure that ^{95}Tc, ^{94}Tc, and ^{93}Tc show higher cross sections than calculated values, while ^{96}Tc shows lower values. From the above observations it can be inferred that the products $^{93-95}Tc$, have contributions from ICF involving the projectile breakup into α and ^{8}Be followed by fusion of ^{8}Be with the target. It is surprising to note that the theoretical excitation function for the ^{96}Tc overestimate the experimental results, thereby showing the negligible effects from the breakup of the projectile ^{12}C. From the breakup fusion model, the disagreement between theoretical and experimental values of the cross sections of ^{96}Tc is attributed to the uncertainty in PACE2 calculations as this isotope is not expected to be formed in ICF process as will be discussed later.

Figure 1(d) shows the excitation functions for the products ^{93}Mo, $^{90,92}Nb$. In case of ^{93}Mo there is fairly good agreement between the experiment and theory indicating its formation in CF process, that is $\alpha p3n$ channel. The contribution from ICF, if any, is not clearly seen in $\sigma(E)$. The measured $\sigma(E)$ for $^{92}Nb^{m}$ agrees with the PACE2 predictions. However $^{92}Nb^{m}$ represents a small fraction of the cross section of ^{92}Nb as the high spin isomer, $^{92}Nb^{g}$ could not be measured owing to its long half-life. Thus the cross section of ^{92}Nb would actually be much higher than PACE2 prediction, indicating the contribution of ICF in the yield of ^{92}Nb. In case of ^{90}Nb, which is the high spin isomer, the measured cross section value accounts for almost the entire cross section of this product. The experimental values are much higher than the PACE2 predictions, indicating that there is a contribution from ICF process.

The present observations indicate that ICF occurs even at as low energy as 6 MeV/nucleon. Similar results were obtained by Parker *et al.* [10] and Vergani *et al.* [24]. The exact mechanism of such ICF reactions is not clearly understood. Several models have been proposed so far [5–8], as discussed earlier, to explain the ICF reaction mechanism. In order to understand the various aspects of the ICF phenomena, it is important to do a detailed study of the role of the entrance-channel angular momentum and mass asymmetry. An interesting question is to what extent this breakup is accompanied by fusion of one of the two fragments of the projectile. The recoil range studies, discussed in the following section, are aimed at addressing this question.

B. Recoil range distributions

Figure 2(a) shows the measured recoil range distributions for the products ^{97}Rh, ^{97}Ru, and ^{95}Ru at the beam energy of 84 MeV. The recoil range distributions of the above products are the simplest, consisting of a well-defined peak at a depth corresponding to the expected recoil range of the ^{101}Rh compound nucleus. The width of these peaks reflects the perturbing effects of the evaporation of nucleons on the recoil velocity of the product, combined with the effects of straggling and finite target thickness. The results of detailed modelling of the recoil range distributions predicted by PACE2 for CF with suitable normalization are shown as the solid curves. This modeling procedure reproduces the distributions reasonably well, thereby confirming the fact that the production of these residues is purely by complete fusion. The above

distributions are also centered approximately around the compound nucleus recoil range. This indicates the absence of ICF in the formation of rhodium and ruthenium isotopes in the system.

Figure 2(b) shows the recoil range distributions of seven residues from the reactions of 84 MeV ^{12}C with ^{89}Y. Whereas the ^{96}Tc distribution consists of a single peak, at the range expected for a residue recoiling with almost the CN velocity, the other products namely, $^{93-95}$Tc, ^{93}Mo, ^{90}Nb, and ^{92}Nb show additional components at a lower range. These components correspond to the two ICF processes, ^{89}Y(^{12}C,α)^{97}Tc* and ^{89}Y(^{12}C,^{8}Be)^{93}Nb*. In these reactions, α and ^{8}Be act essentially as spectators during the reaction, so that the linear momentum transfer of the residue is reduced to 2/3 and 1/3 of the CN value, respectively.

C. Breakup fusion model analysis of the ICF

In Fig. 2(b) the dashed lines are the ICF cross sections obtained by subtracting the simulated RRD's from the experimental RRD's. The low range component clearly reflects incomplete momentum transfer in the ICF process leading to Tc, Mo, and Nb isotopes. The RRD for these ICF products was deduced using the breakup fusion model [5]. The Monte Carlo simulation of RRD was carried out using PACE2 code by supplying the E^* and $\langle l \rangle$ of the incompletely fused composite (IFC) nuclei ^{97}Tc and ^{93}Nb formed in the binary reactions,

$$^{12}\mathrm{C}+^{89}\mathrm{Y}\rightarrow{}^{97}\mathrm{Tc}^*+{}^{4}\mathrm{He},$$

$$^{12}\mathrm{C}+^{89}\mathrm{Y}\rightarrow{}^{93}\mathrm{Nb}^*+{}^{8}\mathrm{Be}.$$

The E^* of the intermediate nucleus (^{97}Tc*) was evaluated using the expression,

$$2/3E_{\mathrm{lab}}(97/101)+Q_{gg}.$$

It was found to be 48.48 MeV for the above system at $E_{\mathrm{lab}}=84$ MeV. The IFC was assumed to have a single spin value equal to 2/3 times the $1_{\max}$ of the entrance channel, which was found to be 30$\hbar$. Likewise the E^* of ^{93}Nb* was evaluated as

$$1/3E_{\mathrm{lab}}(93/101)+Q_{gg}.$$

The calculated value was found to be 21.37 MeV, and the corresponding spin value was taken as 1/3 times the $l_{\max}$, that is 15$\hbar$. The other input parameters were chosen the same way as in the case of PACE2 calculation for the CF process. The deexcitation of these incompletely fused composite nuclei was followed and the RRD's for the Tc, Mo, and Nb isotopes were generated. The simulated RRD's are shown as dotted curves. The simulated RRD's reproduce the deduced RRD's for $^{93-95}$Tc, ^{93}Mo, and ^{92}Nb except for the width which are rather narrow for the simulated RRD's. This can be attributed to the limitations in the simulation as the angular distribution of the outgoing particles is not taken into account. The break up fusion model fails to account for the RRD of ^{90}Nb. This is owing to the fact that the E^* of IFC, (^{93}Nb) formed by fusion of an alpha particle with ^{89}Y is not sufficient for emission of three neutrons to give ^{90}Nb. This shows that ^{90}Nb is not formed by alpha transfer from ^{12}C to ^{89}Y. Instead it may be formed by two proton transfer followed by emission of one neutron.

TABLE II. Contributions of CF and ICF* cross sections (in mb) in the yields of Tc, Mo, and Nb isotopes in 84 MeV ^{12}C on ^{89}Y.

Nuclei	CF	ICF
^{95}Tc^{g}	59.3±5.1	33.8±3.4
^{94}Tc^{g}	66.4±4.4	61.7±6.2
^{93}Tc^{g}	79±3	7.9±0.8
^{93}Mo^{m}	50.4±3.2	13.4±1.4
^{92}Nb^{m}		0.88±0.28
^{90}Nb^{g}		17.3±2.3

Table II shows the ICF cross sections in the yields of Tc, Mo, and Nb isotopes. The relative cross sections of $^{94-95}$Tc was used to deduce the E^* and $\langle l \rangle$ of the IFC and thereby evaluate the angular momenta involved in the ICF. This method of obtaining the angular momentum distribution of a CN from the relative yields of ER's is well established [25]. The E^* and $\langle l \rangle$ of the IFC, ^{97}Tc was varied in the range of 40–50 MeV and 25–35$\hbar$, respectively, and the yields of ^{95}Tc and ^{94}Tc were compared with experimentally deduced ICF cross sections for these products. The best fit with experimental values was found for $E^*=46$ MeV and $\langle l \rangle = 30\hbar$. These values agree with the predictions of breakup fusion model as calculated above. The corresponding angular momentum of entrance channel would be $30\times 3/2=45\hbar$, which agrees with the $l_{\max}$ value (45$\hbar$) calculated using the prescription of Wilczynski [26]. This shows that the ICF process is associated with peripheral collisions. This observation is in agreement with the predictions of sum rule model [7] that the ICF occurs only in peripheral collisions involving $l_{\mathrm{ICF}} > l_{\mathrm{CR}}$ for CF. The CF cross section at 84 MeV beam energy was obtained from the excitation function data measured experimentally in the present work, and taking the cross section of a few stable residues (^{95,96}Ru,^{96}Tc,^{94}Mo) from the PACE2 code. These stable residues contributes only 10–15% of the σ_{CF}. The σ_{CF} value was found to be 1240 ±140 mb. The corresponding l_{CR} deduced from the σ_{CF} value was 38$\hbar$. This value of l_{CR} is in good agreement with the l_{CR} value of 39$\hbar$ calculated using the prescription of Wilczynski [26].

Thus the present study has shown that ICF contributes significantly to the total reaction cross section even at as low energy as 6 MeV/amu in case of low Z heavy ion induced reactions. The study reveals that ICF follows breakup fusion mechanism in which the projectile breaks into the fragments ($\alpha+{}^{8}$Be). Subsequently either of the two fragments can fuse with the target nucleus bringing in the angular momenta in the ratio of its mass to that of the projectile. The calculation of the $\langle l \rangle$ of the IFC formed in ICF from the relative yields of the $^{94-95}$Tc isotopes corroborates the peripheral nature of collision leading to ICF.

V. CONCLUSION

Excitation functions of twelve evaporation residues were measured in the ^{12}C+^{89}Y system in the beam energy range 70–87 MeV. RRD's of ER's were also measured at 84 MeV.

Comparison of the excitation functions with the Monte Carlo simulation code suggests that there is a significant enhancement in the cross section of the α emission products, such as $^{93-95}$Tc in this system, thereby indicating the contribution of ICF processes. The simulation of RRD's indicates significant contribution of ICF in the Tc, Mo, and Nb products. The ICF formation of Tc, Mo, and ^{92}Nb has been explained in terms of the breakup of ^{12}C into $\alpha+^{8}$Be followed by fusion of either of them with the target. However, the model fails to explain the ICF in ^{90}Nb product. This may be attributed to the formation of this product by the transfer of two protons from projectile to the target followed by neutron emission. The average angular momentum of the intermediate nucleus formed in ICF was deduced from the relative yields of the ICF products. The results corroborate the peripheral nature of the ICF.

ACKNOWLEDGMENTS

The authors thank Shri. D. C. Ephraim for preparing the thin metal foils and the operating crew of the PELLETRON facility for their help in carrying out the irradiations. One of the authors (S.M.) thanks Nuclear Science Centre, New Delhi for financial help through a UFUP project. Another author (B.B.) thanks the Council of Scientific and Industrial Research for financial support.

[1] Ch. Ngo, Prog. Part. Nucl. Phys. **16**, 139 (1985).
[2] H. C. Britt and A. R. Quinton, Phys. Rev. **124**, 877 (1964).
[3] J. Galin, B. Gatty, D. Guirean, C. Rousset, V. C. Schlotthauer-Voos, and X. Tarrago, Phys. Rev. C **9**, 1126 (1974).
[4] T. Inamura, M. Ishihara, T. Fakuda, T. Shimoda, and H. Hiruta, Phys. Lett. **68B**, 51 (1977).
[5] T. Udagawa and T. Tamura, Phys. Rev. Lett. **45**, 1311 (1980).
[6] M. I. Sobel, P. J. Siemens, J. P. Bondorf, and H. A. Bethe, Nucl. Phys. **A251**, 502 (1975).
[7] J. Wilczynski, K. Siwek-Wilczynska, J. Van Driel, S. Gonggrijp, D. C. J. M. Hageman, R. V. F. Janssens, J. Lukasiak, R. H. Siemssen, and S. Y. Van der Werf, Nucl. Phys. **A373**, 109 (1982).
[8] J. P. Bondorf, J. N. Dey, G. Fai, A. O. T. Karvinen, and J. Randrup, Nucl. Phys. **A333**, 285 (1980).
[9] M. Blann, Phys. Rev. C **31**, 1245 (1985).
[10] D. J. Parker, J. J. Hogan, and J. Asher, Phys. Rev. C **39**, 2256 (1989).
[11] H. Morgenstern, W. Bohne, W. Galster, and K. Grabisch, Z. Phys. A **324**, 443 (1986).
[12] I. Tserruya, V. Steiner, Z. Fraenkel, P. Jacobs, G. D. Kovar, W. Henning, M. F. Vineyard, and B. G. Glagola, Phys. Rev. Lett. **60**, 14 (1988).
[13] B. S. Tomar, A. Goswami, A. V. R. Reddy, S. K. Das, P. P. Burte, S. B. Manohar, and Satya Prakash, Z. Phys. A **343**, 223 (1992).
[14] B. S. Tomar, A. Goswami, A. V. R. Reddy, S. K. Das, P. P. Burte, S. B. Manohar, and Bency John, Phys. Rev. C **49**, 941 (1994).
[15] H. Morgenstern, W. Bohne, K. Grabish, D. G. Kovar, and H. Lehr, Phys. Lett. **113B**, 463 (1982).
[16] W. Trautmann, Ole Hansen, H. Tricoire, W. Hering, R. Ritzka, and W. Trombik, Phys. Rev. Lett. **53**, 1630 (1984).
[17] H. Tricoire, C. Gerschel, N. Perrin, H. Sergolle, L. Valentin, D. Bachelier, H. Doubre, and G. Gizon, Z. Phys. A **306**, 127 (1982).
[18] A. Gavron, Phys. Rev. C **21**, 230 (1980).
[19] L. C. Northcliffe and R. F. Schilling, At. Data Nucl. Data Tables **A7**, 233 (1970).
[20] U. Reus and W. Westmeier, At. Data Nucl. Data Tables **29**, 1 (1983).
[21] S. K. Kataria, V. S. Ramamurthy, and S. S. Kapoor, Phys. Rev. C **18**, 549 (1978).
[22] C. M. Perey and F. G. Perey, At. Data Nucl. Data Tables **17**, 1 (1976).
[23] P. M. Endt, At. Data Nucl. Data Tables **26**, 47 (1981).
[24] P. Vergani, E. Gadioli, E. Vaciago, E. Fabrici, E. Gadioli Erba, and M. Galmarini, Phys. Rev. C **48**, 1815 (1993).
[25] M. Dasgupta, A. Navin, Y. K. Agarwal, C. V. K. Baba, H. C. Jain, M. L. Jhingan, and A. Roy, Phys. Rev. Lett. **66**, 1414 (1991).
[26] J. Wilczynski, Nucl. Phys. **A216**, 386 (1973).